

Theory of Optical Pump THz Probe with sub-picosecond time-dependent material properties: the Perturbative Transfer Matrix Method

Yingshu Yang,¹ Stefano Dal Forno,¹ and Marco Battiato^{1,*}

¹*School of Physical and Mathematical Sciences, Nanyang Technological University, Singapore, Singapore*
(Dated: June 3, 2022)

Optical Pump THz Probe (OPTP) is a technique by which an optical subpicosecond laser pulse is used to trigger ultrafast dynamics in a target multilayered film, and a THz pulse is sent with variable delay to probe the status of the system. For a slowly varying dielectric response, the non-equilibrium THz response can be described using a quasi-static description and hence standard transfer matrix methods (TMM) can be employed. However, if the non-equilibrium timescale is similar to or shorter than the THz probe time width, there are currently no available theoretical tools to describe this situation. We develop a theoretical framework, the Perturbative Transfer Matrix Method (PTMM), to fill in this gap. The full time dependence of the properties of the materials, as well as the proper propagation via Maxwell's equations, are correctly accounted for. We observe that, while slowly varying material properties produce an OPTP signal which can very well be interpreted within the quasi-static limit when the excitation dynamics are fast, that approximation cannot account for crucial features of the OPTP signal. The fast excitation timescale produces a significant broadening of the OPTP signal. We show that not only OPTP can be used to extract the sub-picosecond timescale of the excitation, but it also provides a sub THz period resolution, and dynamics as fast as a few hundreds of femtoseconds can be distinguished even with narrowband THz pulses with time durations as long as many picoseconds.

Terahertz time-domain spectroscopy (THz-TDS) is an attractive experimental method that uses a frequency range between 0.1 THz to 10 THz to measure and extract dielectric properties of materials such as permittivities and refractive indices. This method exploits the fact that electric fields are measured in the time domain and does not rely on simple intensity measurements¹.

Thus, THz-TDS is often used for the measurement of THz responses of materials in the steady state. Additionally, based on the optically gated emission and detection technique together with the time domain measurement of THz pulse in THz-TDS, another experimental method – Optical Pump Terahertz Probe (OPTP) – has been developed and is currently widely used for the measurement and study of non-equilibrium condition material properties, such as charge carrier dynamics and mobilities²⁻⁴.

In OPTP experiments, the optical pump drives the system into a strong out-of-equilibrium state. Subsequently, a THz probe is sent onto the sample to investigate its properties. In this excited state, a number of ultrafast processes can be triggered: THz emission⁵⁻⁸, ultrafast laser induced demagnetization⁹⁻¹³, superdiffusive spin transport^{14,15}, coherent magnetic precession¹⁶⁻¹⁸, and laser induced phase transitions^{19,20}. The application of the OPTP experimental technique provides in-depth analysis of these processes as well as information on the non-equilibrium status of materials such as semiconductors, superconductors and metals, and other interesting materials such as, Mxenes²¹, perovskites²², MoS_2 ²³, graphene^{3,24,25}, topological insulators²⁶, which are all important component to computers, lasers, light-emitting devices, electrodes, information storage devices, and future electronic devices^{2,27}.

Typically, THz-TDS experiments are performed in multilayered system where the THz probe is used to

access the equilibrium properties of a specific layer of the sample. However, in the case of OPTP, the optical pump drives the system to a strong out-of-equilibrium state. The material undergoes a sub-picosecond excitation and the subsequent relaxation produces dynamics in the picosecond or subpicosecond regime. In this case the responses to the electromagnetic radiation are not anymore invariant with time translation.

The Transfer Matrix Method (TMM) (or transfer function), is a basic and mature method for the theoretical study of electromagnetic wave propagation in multilayer structures²⁸. However, the TMM is restricted to describe the propagation of electromagnetic (EM) waves in systems at equilibrium, where the dielectric response of the material varies on a slower time scale than the period of the probe. Within this approximation one can define a time and frequency dependent dielectric response function, where the slow time variation is accounted by the explicit time dependence, while the high frequency contributions are modelled within the Fourier domain. Notice that this approach requires a clear separation of the slow timescale related to the evolution of the out-of-equilibrium dynamics of the materials and a fast timescale related to the period of the used probe radiation. Methods, based on this approximation have been developed and applied to the extraction of slowly time-dependent conductivity and susceptibility for ultrafast far-infrared dynamics²⁹⁻³¹ as well as layered systems³².

However, that approximation fails in the case of OPTP. The frequency of the probe and the time evolution dynamics timescales are completely overlapping. This causes even the interpretation of the results as a time-varying dielectric response to lose meaning, as spectral features typical of the time-evolution of the excited system are expected to appear within the spectrum of the

transmitted or reflected THz radiation. The problem becomes more complex and the interaction of the radiation with materials with time-varying properties must be described in more detail.

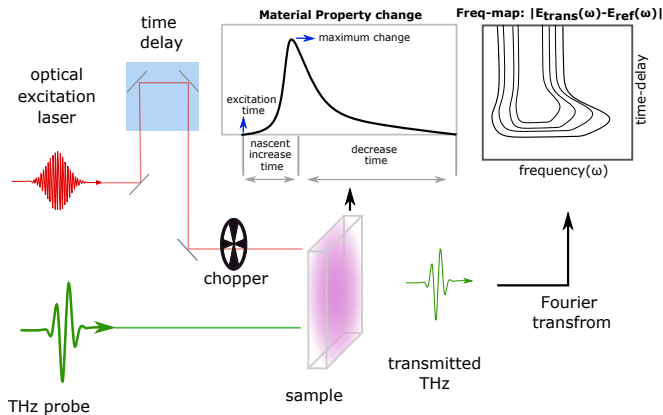


Figure 1. Concept figure: A description of the OPTP setup and the PTMM recipe. The frequency map is the spectrum difference between the transmitted THz probe through a non-excited and excited sample with different time delay.

To address this challenge we extend the TMM method using perturbation theory. We describe the dielectric response of the material using a time-dependent generalised Drude function. We explicitly account for the out-of-equilibrium carrier densities and scattering rates induced by the optical pump. With this, our Perturbative Transfer Matrix method (PTMM) is capable of solving Maxwell's equations for a strongly excited multilayered system. We also calculate the frequency map of the pump-on pump-off spectrum difference of the transmitted THz probe (Fig. 1) and demonstrate that an accurate analysis of the OPTP spectrum can provide sub-period time resolution (less than 100 fs) into the sample's dynamics. In particular, this allows for OPTP to resolve not only slow dynamics but even the very fast excitation process, which often takes only a few hundreds of fs for ferromagnets like Ni^{10,11,13} and Fe^{33,34} and for noble metals like Au³⁵⁻³⁷.

The article is organised as follows: First, we introduce the Maxwell-Drude system and expand it in perturbation orders. Second, we briefly recap the application of the TMM to the 0-th order. Third, we proceed to develop an extension to the TMM, the PTMM to obtain an analytic expression of the 1-st order. We then construct the analytic expression of the OPTP spectra in transmission and reflection. Finally, we apply our developed method to simulate two types of time-resolved spectral maps to study the sub-period dynamics of excited multilayers.

I. PERTURBATION EXPANSION OF THE MAXWELL-DRUDE SYSTEM

We first address the case of radiation within a uniform material with material properties changing with

time as a result of a femtosecond laser excitation and subsequent thermalisation. We assume that the frequency ω -dependent total permittivity $\epsilon_T[\omega]$ of the material can be written as the sum of a Drude component $\epsilon_D[\omega]$ and a remaining background component $\epsilon_B[\omega]$, which accounts for all the non-Drude contributions (e.g. the interband transitions) with a generic frequency dependence. We further assume that the background component of the permittivity is not modified by the laser. Conversely, we will allow the Drude parameters to be explicitly time-dependent.

The above situation for a single linear polarisation of the electric E and magnetic H fields propagating along the z axis is described by the Maxwell-Drude system (where we have taken the Fourier transform in time t , but not in space, of the Faraday's and Ampere's laws):

$$\begin{aligned} \partial_z E[z, \omega] &= -i\omega\mu[\omega]H[z, \omega], \\ \partial_z H[z, \omega] &= -i\omega\epsilon_B[\omega]E[z, \omega] + J[z, \omega], \\ \partial_t J[z, t] &= -\gamma J[z, t] + \frac{ne^2}{m}E[z, t], \end{aligned} \quad (1)$$

where μ is the permeability of the medium, $J[z, t]$ is the current density (along the same direction as the electric field) induced by the Drude response, e is the electron charge, and m the effective mass, n is the number of carriers, and γ the inverse scattering lifetime. Notice that we have not taken the Fourier transform of the last equation. We take the chance to highlight that the system of equations is homogeneous.

In the case n and γ are constant in time, the last equation leads to the known expression for the Drude conductivity,

$$\sigma_D[\omega] = \frac{ne^2}{m(\gamma - i\omega)}, \quad (2)$$

corresponding to a total permittivity $\epsilon_T[\omega]$ (i.e. including the background contribution and the Drude contribution) of

$$\epsilon_T[\omega] = \epsilon_B[\omega] + i\frac{\sigma_D[\omega]}{\omega}. \quad (3)$$

We now treat the case where the number of carriers n and the inverse Drude scattering lifetime γ instead have a generic dependence on time. An increase in the number of carriers in time can, for instance, describe the transient photodoping of a semiconductor during a femtosecond laser excitation, while its decrease could be due to the subsequent carrier recombination. On the other hand, a change in γ can, for instance, describe the increased number of scatterings triggered by the increased phonon temperature after an excitation. We write the Drude parameters as the sum of their equilibrium values, $\gamma^{[0]}$ and $n^{[0]}$, and a time-dependent part, $\gamma^{[1]}$ and $n^{[1]}$,

$$\gamma[z, t] = \gamma^{[0]} + \gamma^{[1]}[z, t], \quad (4)$$

$$n[z, t] = n^{[0]} + n^{[1]}[z, t]. \quad (5)$$

Notice that we allow for the variations to be also position-dependent. However, for shortness, we will suppress the explicit position dependence throughout the rest of this section as it does not play any role. We will recover it explicitly in the next section.

If we assume that the time variations are small, we can write the fields and the current up to the first perturbative order as,

$$\begin{aligned} E[z, t] &\approx E^{[0]}[z, t] + E^{[1]}[z, t], \\ H[z, t] &\approx H^{[0]}[z, t] + H^{[1]}[z, t], \\ J[z, t] &\approx J^{[0]}[z, t] + J^{[1]}[z, t], \end{aligned} \quad (6)$$

where the two orders must satisfy two different sets of equations. Before proceeding let us stress here the crucial point of this approach: the perturbative expansion does not impose any requirement for the variations to be slow. This is critical since we aim at addressing the case where the material properties are changing over a similar timescale as the THz radiation's period.

The 0-th order satisfies the unperturbed Maxwell-Drude system Eqs. 1, with constant equilibrium Drude parameters. This set of equations can be solved analytically within a multilayer using standard approaches like the Transfer Matrix Method³⁸. We assume the 0-th order solved (we will explicitly write the expression in the next section), and focus on the 1-st order set of equations. We address explicitly only the case of a time-varying Drude scattering rate (the generalisation is straightforward),

$$\begin{aligned} \partial_z E^{[1]}[z, \omega] &= -i\omega\mu[\omega]H^{[1]}[z, \omega], \\ \partial_z H^{[1]}[z, \omega] &= -i\omega\epsilon_B[\omega]E^{[1]}[z, \omega] + J^{[1]}[z, \omega], \\ \partial_t J^{[1]}[z, t] &= -\gamma^{[0]}J^{[1]}[z, t] + \frac{n^{[0]}e^2}{m}E^{[1]}[z, t] - \gamma^{[1]}J^{[0]}[z, t]. \end{aligned} \quad (7)$$

We can observe that, different from Eqs. 1, this system of equations is not homogeneous, and the last term in the first order Drude equation acts as a source term.

We now take the Fourier transform of the last of Eqs. 7, and reduce the system to the Maxwell's equations,

$$\begin{aligned} \partial_z E^{[1]}[z, \omega] &= -i\omega\mu[\omega]H^{[1]}[z, \omega], \\ \partial_z H^{[1]}[z, \omega] &= -i\omega\epsilon_T[\omega]E^{[1]}[z, \omega] + \mathcal{J}[z, \omega], \end{aligned} \quad (8)$$

with a source term,

$$\mathcal{J}[z, \omega] = \sigma_D^{[0]}[\omega] \mathcal{F} \left[-\frac{m\gamma^{[1]}[t]}{n^{[0]}e^2} J^{[0]}[z, t], \omega \right], \quad (9)$$

which has the dimensionality of a volume current.

In case both the Drude scattering rate and the Drude carrier density are time dependent, the expression in Eqs. 8 remains the same, with a source which now includes another term,

$$\begin{aligned} \mathcal{J}[z, \omega] &= \sigma_D^{[0]}[\omega] \\ &\times \mathcal{F} \left[\frac{n^{[1]}[t]}{n^{[0]}} E^{[0]}[z, t] - \frac{m\gamma^{[1]}[t]}{n^{[0]}e^2} J^{[0]}[z, t], \omega \right]. \end{aligned} \quad (10)$$

For later convenience, we express the source in terms of its spatial Fourier transform:

$$\mathcal{J}[z, \omega] = \sum_l \mathcal{J}[k_l, \omega] \exp[ik_l z]. \quad (11)$$

So far we have only described how to treat the effect of time-varying Drude material parameters on Maxwell's equations within a single material. We have found that by expanding the electric and magnetic fields in orders of the time-dependent correction to the equilibrium Drude parameters, the 0-th order satisfies the standard Maxwell's equations, while the 1-st order the non-homogeneous Eqs. 8. In the following section, we will see how to apply them to a multilayer system and how to describe an OPTP experiment.

II. PERTURBATIVE TRANSFER MATRIX METHOD

We address the propagation of electromagnetic radiation through a multilayer at normal incidence. We count layers from left to right starting from 1 up to the number of layers N . We assume the multilayer system to be sandwiched by air. Below we will treat the air on the left and on the right of the sample as semi-infinite layers and assign the index 0 to the air on the left and $N + 1$ to the air on the right. We further assume all layers' thicknesses d_n to be known. To address the case of propagation through a multilayer, one typically solves the Maxwell's equations independently within each layer using the local material's properties and then enforces the appropriate field continuity equations at the interfaces.

The case of materials with time-dependent material properties is handled in a similar way, with two important differences. The propagating radiation is the sum of a 0-th and a 1-st order component within each layer. Within each layer, the four fields (electric and magnetic, 0-th and 1-st) satisfy four equations, of which the last two are Eqs. 8 and involve both the 0-th and the 1-st order. The first two instead involve only the 0-th order components and are the standard Maxwell's equations within the multilayer. For this reason, we first solve the propagation of the 0-th order component using standard techniques, and only after the expression for the 0-th order component is known, we can proceed with solving Eqs. 8.

A. 0-th order propagation

For the 0-th order, we follow the textbook TMM (a derivation with symbols consistent with this article can be found in Ref. 38). We report below the main TMM results for the reader's convenience and to make the extension to PTMM easier to follow. Within a given layer n the 0-th order electric and magnetic field can be expressed as a multiplication of a 2×2 matrix and a vector

containing the amplitudes of the right $f_n^{[0]>}$ and left $f_n^{[0]<}$ propagating waves:

$$\begin{bmatrix} E_n^{[0]} \\ H_n^{[0]} \end{bmatrix} [\omega, z] = \bar{a}_n [\omega, z] \begin{bmatrix} f_n^{[0]>} \\ f_n^{[0]<} \end{bmatrix} [\omega], \quad (12)$$

where

$$\bar{a}_n [\omega, z] = \begin{bmatrix} e^{i\omega\sqrt{\epsilon_n\mu_n}z} & e^{-i\omega\sqrt{\epsilon_n\mu_n}z} \\ -\sqrt{\frac{\epsilon_n}{\mu_n}} e^{i\omega\sqrt{\epsilon_n\mu_n}z} & \sqrt{\frac{\epsilon_n}{\mu_n}} e^{-i\omega\sqrt{\epsilon_n\mu_n}z} \end{bmatrix}. \quad (13)$$

By requiring appropriate continuity equations to the fields at the interfaces between layers, one finds that the field amplitudes at the two air layers to the left and the right of the sample are linked by,

$$\begin{bmatrix} f_{N+1}^{[0]>} \\ f_{N+1}^{[0]<} \end{bmatrix} = \bar{T}_{[0,N+1]} \begin{bmatrix} f_0^{[0]>} \\ f_0^{[0]<} \end{bmatrix}, \quad (14)$$

where $\bar{T}_{[0,N+1]}$ is the Transfer Matrix with a generalised form,

$$\bar{T}_{[n,m]} = \bar{a}_m^{-1} [0] \left(\prod_{j=m-1}^{n+1} \bar{a}_j [d_j] \bar{a}_j^{-1} [0] \right) \bar{a}_n [0]. \quad (15)$$

B. 1-st order propagation

On the other hand, the set of equations Eqs. 7 cannot be solved using the TMM, since the equations are not homogeneous, and a source term is present.

We first construct the general solution to Eqs. 7. We obtain that the 1-st order corrections to the fields within a given layer n as,

$$\begin{bmatrix} E_n^{[1]} \\ H_n^{[1]} \end{bmatrix} [\omega, z] = \bar{a}_n [\omega, z] \bar{f}_n [\omega] + \sum_l \mathcal{J}_n [k_l, \omega] \bar{b} [\omega, k_l, z]. \quad (16)$$

For the full derivation of the expression above and the definition of \bar{b} refer to Appendix A.

Without loss of generality, we can assume that only the layer M has time-dependent properties. The general case can be constructed as the summation of 1-st order corrections due to all the layers that present time-dependent properties. Using the expression in Eq. 16, the field continuity conditions at all the layers' interfaces can be written. We obtain that the wave intensities in any two layers $n < M$ and $m > M$ are linked by the expression,

$$\begin{bmatrix} f_m^{[1]>} \\ f_m^{[1]<} \end{bmatrix} = \bar{T}_{[n,m]} \begin{bmatrix} f_n^{[1]>} \\ f_n^{[1]<} \end{bmatrix} + \sum_l \mathcal{J} [k_l, \omega] \bar{T}_{[M,m]} \times (\bar{a}_N^{-1} [d_N] \bar{b} [\omega, k_l, d_N] - \bar{a}_N^{-1} [0] \bar{b} [\omega, k_l, 0]), \quad (17)$$

where $\bar{T}_{[n,m]}$ has the same expression as shown in Eq. 15. For simplicity, considering the two semi-infinite air layers, Eq. 17 can be written as,

$$\begin{bmatrix} f_{N+1}^{[1]>} \\ f_{N+1}^{[1]<} \end{bmatrix} = \bar{T}_{[0,N+1]} \begin{bmatrix} f_0^{[1]>} \\ f_0^{[1]<} \end{bmatrix} + \begin{bmatrix} J_M^> \\ J_M^< \end{bmatrix}. \quad (18)$$

The above Eq. 17 can be used to calculate, for instance, transmitted and reflected waves (more on this below) and, after that, the amplitudes of right and left moving waves in any layer.

C. Reflection and transmission through excited layers

We are now ready to compute the reflection and transmission. For the 0-th order, the approach is the textbook one. Assuming that the THz probe is incident from the left, we substitute in Eq. 14 $f_0^{[0]>}$ with the temporal shape of the incoming probe, and $f_{N+1}^{[0]<}$ with 0 to signify that no wave is sent towards the sample from the right. Solving the two equations for $f_{N+1}^{[0]>}$ and $f_0^{[0]<}$ will provide the shape of the transmitted and the reflected waves, respectively³⁸.

We are however interested in the changes to the reflected and transmitted waves due to the time-varying properties in the sample. Eq. 17 works in particular for the semi-infinite air layers on the left and on the right. We need to substitute $f_0^{[1]>}$ and $f_{N+1}^{[1]<}$ with 0, since the time-dependence of the material's properties, obviously, induces no variation to the incoming THz probe on the left or the absence of incoming radiation from the right. Eq. 18 reduces to two equations for $f_{N+1}^{[1]>}$ and $f_0^{[1]<}$, that are respectively the correction to transmitted and reflected waves.

The correction to the transmission is:

$$f_{N+1}^{[1]>} = J_M^> - \frac{\bar{T}_{[0,N+1],12}}{\bar{T}_{[0,N+1],22}} J_M^<, \quad (19)$$

where the further subscriptions of $\bar{T}_{[0,N+1]}$ refer to the matrix elements. For the reader's convenience we have summarised and collected all the expressions required for the application of the PTMM in Appendix B.

III. RESULTS

We now apply the approach developed above to an example: the computation of the propagation of a THz wave through a multilayer. We use the same experimental THz profile as in Ref. 38, as a probe incoming from the left. We compute the propagation through a quartz(1mm)/Ti(8nm) sample. We construct the dielectric response for quartz at equilibrium by using a frequency-independent refractive index of $2.01 + 0i$,^{39,40}

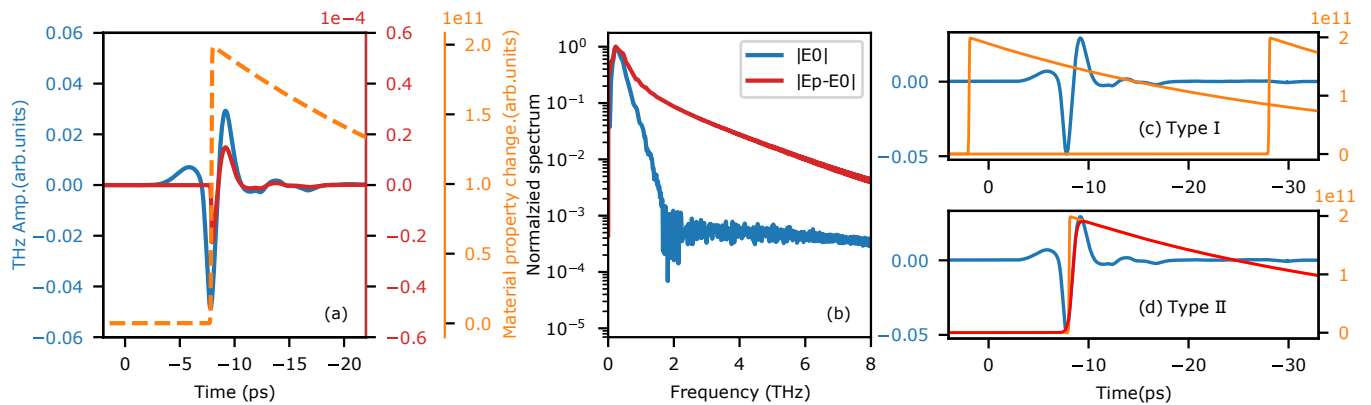


Figure 2. A simple description of the two type of testings. (a) A comparison between the transmitted probe through non-excited system $|E_0|$ and the 1-st order change $|E_p - E_0|$ pulse and the influence of the material property change on the $|E_p - E_0|$ pulse shape (again, not in scale). (b) The normalized spectrum of $|E_0|$ and $|E_p - E_0|$ (notice that the two spectra are not in scale with each other). (c) Testing type I: The excitation pulse and the THz probe is sent at different time delays, so that the material property function with a fixed increase time can be considered as scanning over the full THz pulse. (d) Testing type II: The excitation pulse and the THz pulse are sent at a fixed time delay when the excitation time is overlapping with the central time position of the THz pulse. The increase time of the material property function is changed from 80fs (orange) to 800fs (red). (Note: All blue and red axes are THz amplitude in arbitrary units while not in the same scale. All orange axes represent the material property change.)

(yet notice that the software works for generic frequency-dependent material's properties). We do not add any Drude contribution for quartz. We assume that Ti's response to the electric field is purely Drude-like: we construct the number of carriers n and the Drude scattering rate γ at equilibrium by using a plasma and damping frequency taken as 7.29eV and 0.082eV respectively⁴¹. No further contributions to the response of Ti at equilibrium have been considered (yet, again, a further contribution to the dielectric function with a generic frequency-dependence can be included).

The changes in the materials' properties due to an optical excitation are supposed to be known before computing the propagation of the probe pulse. The method above can address only changes that can be approximated as modifications of Drude parameters (meaning that bleaching of inter-band transitions is beyond the proposed approach). An increase in the number of carriers is what is expected to dominate in semiconductors irradiated with a frequency above the optical bandgap. On the other hand, an increase in the scattering rate is what is to be expected of excited metals, where the increase in the phononic temperature acts as a temporary reduction of conductivity. Nonetheless, the proposed approach can handle all intermediate cases as well and can be used to characterise the out-of-equilibrium behaviour of a material using OPTP.

In the example at hand, for simplicity, we ignore the effect of the optical laser excitation on quartz and assume that Ti experiences an increase $\gamma^{[1]}(t)$ in its Drude scattering rate in the form,

$$\delta\gamma(t) = h \frac{e^{-\frac{t-t_0}{b}}}{e^{-\frac{(t-t_0)-a/2}{a/4}} + 1}, \quad (20)$$

where h controls the maximum scattering rate change, a is the increase time and b is the following decrease time, t_0 is the time position of the excitation.

The effect of the non-equilibrium is shown in Fig. 2(a) and (b). We here refer the transmitted probe through a non-excited system as E_0 (blue in Fig. 2(a)) and an excited system as E_p . Thus, $E_p - E_0$ (red in Fig. 2(a)) is the first-order change of the transmitted probe. And the orange line refers to the scattering rate $\gamma^{[1]}(t)$ change. In Fig. 2(b) one can observe that the transmitted wave at equilibrium has relatively a narrow spectrum. On the other hand, when the scattering rate is assumed to be time-dependent (orange line) the first-order correction ($E_p - E_0$) to the transmission shows a much broadened spectrum (see Fig. 2(b)). One can observe that, for the parts of the THz probe which overlap with the slowly changing scattering rate, the correction retains a similar shape to the transmitted probe. However, the part of the probe that overlaps with times when the scattering rate changes sharply, produces a 1-st order correction which gains the temporal features of the dynamics of the non-equilibrium state broadening the spectrum. This is a very promising feature that rises the hope of increasing the time-sensitivity of the OPTP technique below the period of the employed THz radiation. One can further observe that, as expected, the correction has the same sign as the probe signal, since the increase of the scattering rate decreases the conductivity and therefore increases the transmission.

In order to address this aspect, we perform two types of analysis. In the first type (Type I) we will maintain the temporal shape of $\gamma^{[1]}(t)$ and vary the time delay between the optical pump and the THz probe, with the aim of analysing how sensitive OPTP is to the excited

state of the system. For Type II analysis, we will keep the delay constant and change the rise time of the perturbation $\gamma^{[1]}(t)$, with the aim of testing the lowest time resolution achievable with this technique. A schematic description of these two types of testings is shown in Fig. 2 (c) and (d). Fig. 2 (c) shows the two extremes of the delay between the probe (blue line) and the pump. The orange line shows the time evolution of the Drude scattering rate: its time position is linked to the optical excitation time position. Fig. 2 (d) shows the case of a very fast increase of the scattering rate, compared to a slower dynamics: we will analyse the differences in the OPTP signal to study what is the fastest dynamics that can be resolved.

We perform a set of calculations based on Type I analysis. We vary the time delay between the optical pump and THz probe for four cases of dynamics with an increasing rise time of the scattering rate (100fs, 200fs, 300fs, and 400fs) and generate a spectrum map of the OPTP signal (change in transmitted electric field with pump-on and pump-off) as shown in Fig. 3. We observe that the spectral maps show quantitative differences when the out-of-equilibrium dynamics (increase time of $\gamma^{[1]}(t)$) of the system changes. The effect is strongest when the time position of the optical pump and the THz probe overlap within the time width of the THz pulse. We can clearly observe a pronounced broadening of the OPTP spectrum with faster non-equilibrium dynamics. The widest broadening happens at around -8ps, which is when the pump pulse overlaps with the central position time of the probe.

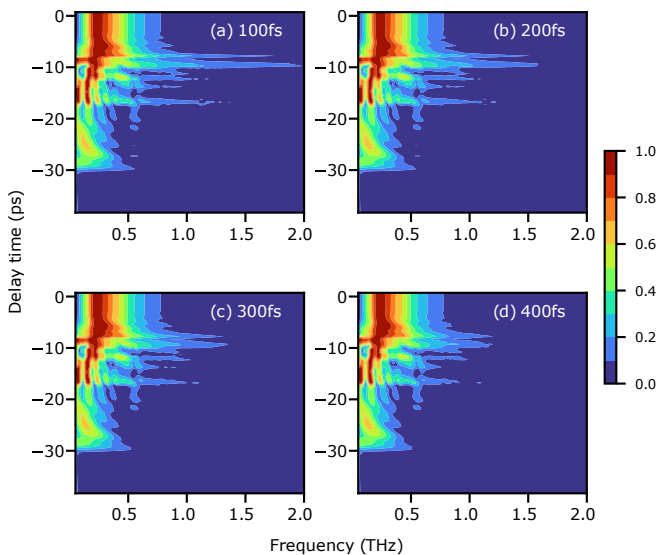


Figure 3. The normalized frequency maps of $|E_p - E_0|$ when the material property function with increase time of 100fs, 200fs, 300fs and 400fs is scanning through the THz probe (the time delay between the excitation laser and THz probe is changing).

We now perform Type II analysis to try to extract some systematic dependence of the spectral width of the

OPTP spectrum on the rise time of the Drude scattering rate. We fix the optical pump THz probe delay time at the delay that shows approximately the maximal spectral width (-8 ps). Then we change the rise time of the Drude scattering rate from 80fs to 800fs and produce a new frequency map as shown in Fig. 4. In this new map, we can more clearly see how faster non-equilibrium dynamics lead to broader spectral features in the OPTP signal. We observe that the inverse of frequency at which the spectrum reaches 1% of its maximum for each increase time (red dotted line in Fig. 4 and inset) is a good indication of the increase time. The increase time and the frequency of the probe scale with an inverse proportionality for points of equal spectral intensity. Specifically, when the intensity of the transmitted THz is 1% of the total, the proportionality is close to $1/\omega$ (as shown in Fig. 4 inset). This is indeed a very interesting feature since a very simple operation can lead to a reasonable estimation of the material's properties ultrafast modification time under laser irradiation. Notice that this analysis does not require performing calculations, and can be conducted directly on the experimental results.

The above-mentioned correspondence, although very convenient due to its simplicity, is not perfect, as can be observed from the inset in Fig. 4. For an accurate extraction of the excitation time, a comparison between experiments and theory is needed. It is however important to note how the method can clearly resolve timescales (hundreds of fs) that are far shorter than the period and the time width of the employed radiation (≈ 5 ps).

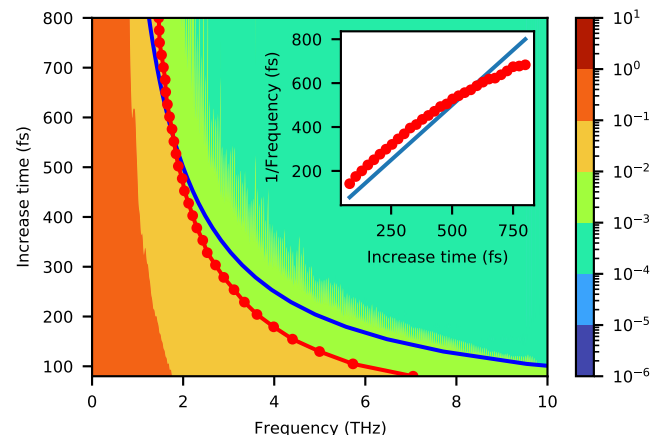


Figure 4. A Normalized frequency map of testing Type II, where the excitation time delay is fixed at the central position of the THz probe (-8 ps) and the increase time of the material property function increases from 80 fs to 800 fs. The red dotted line on the map represents the frequency width of 1% of the maximum spectrum amplitude. The blue line is increase time vs. $1/\text{increase time}$. Inset: The inverse plotting of the extracted red dotted line and blue line on the map. The relationship between $1/\text{frequency-width}$ and increase time. Red dotted line: increase time vs. $1/\text{frequency}$. Blue solid line: increase time vs. increase time.

IV. CONCLUSION

We have constructed a theoretical treatment that can describe the propagation of a THz pulse through a material with Drude properties changing in time over a timescale shorter or comparable to the probe period and time-width. To do that we had to go beyond the approximation of quasi-static changes in material properties. Such treatment allowed us to observe spectral features of the time evolution of the material's properties being transferred to the OOTP signal. The analysis of

these emerging spectral features allows for the extraction of timescales well below the commonly assumed time resolution of the OOTP technique. We have, in particular, suggested a very simple analysis of the spectral features of the OOTP signal that gives a reasonable approximation of the excitation time of a material, without requiring a direct comparison of experiment and theory. Yet it is clear that such comparison can lead to much more precise estimations.

These results show how the OOTP technique can reveal a range of information regarding the ultrafast time evolution of out-of-equilibrium states in materials that has been so far neglected.

-
- * marco.battiato@ntu.edu.sg
- ¹ C. A. Schmuttenmaer, *Chemical Reviews* **104**, 1759 (2004).
 - ² R. Ulbricht, E. Hendry, J. Shan, T. F. Heinz, and M. Bonn, *Reviews of Modern Physics* **83**, 543 (2011).
 - ³ P. A. George, J. Strait, J. Dawlaty, S. Shivaraman, M. Chandrashekhar, F. Rana, and M. G. Spencer, *Nano letters* **8**, 4248 (2008).
 - ⁴ J. H. Strait, H. Wang, S. Shivaraman, V. Shields, M. Spencer, and F. Rana, *Nano letters* **11**, 4902 (2011).
 - ⁵ T. Seifert, S. Jaiswal, U. Martens, J. Hannegan, L. Braun, P. Maldonado, F. Freimuth, A. Kronenberg, J. Henrizi, I. Radu, E. Beaupaire, Y. Mokrousov, P. M. Oppeneer, M. Jourdan, G. Jakob, D. Turchinovich, L. M. Hayden, M. Wolf, M. Münzenberg, M. Kläui, and T. Kampfrath, *Nature Photonics* **10**, 483 (2016), number: 7 Publisher: Nature Publishing Group.
 - ⁶ M. C. Hoffmann, K.-L. Yeh, J. Hebling, and K. A. Nelson, *Opt. Express* **15**, 11706 (2007).
 - ⁷ G. Matthäus, T. Schreiber, J. Limpert, S. Nolte, G. Torosyan, R. Beigang, S. Riehemann, G. Notni, and A. Tünnermann, *Optics communications* **261**, 114 (2006).
 - ⁸ T. Kampfrath, M. Battiato, P. Maldonado, G. Eilers, J. Nötzold, S. Mährlein, V. Zbarsky, F. Freimuth, Y. Mokrousov, S. Blügel, *et al.*, *Nature nanotechnology* **8**, 256 (2013).
 - ⁹ K. Carva, M. Battiato, and P. M. Oppeneer, *Physical Review Letters* **107**, 207201 (2011), publisher: American Physical Society.
 - ¹⁰ M. Battiato, K. Carva, and P. M. Oppeneer, *Physical Review Letters* **105**, 027203 (2010), publisher: American Physical Society.
 - ¹¹ A. Eschenlohr, M. Battiato, P. Maldonado, N. Pontius, T. Kachel, K. Holldack, R. Mitzner, A. Föhlisch, P. M. Oppeneer, and C. Stamm, *Nature Materials* **12**, 332 (2013).
 - ¹² G. Zhang and W. Hübner, *Physical review letters* **85**, 3025 (2000).
 - ¹³ E. Beaupaire, J.-C. Merle, A. Daunois, and J.-Y. Bigot, *Physical Review Letters* **76**, 4250 (1996).
 - ¹⁴ M. Battiato, K. Carva, and P. M. Oppeneer, *Physical Review B* **86**, 024404 (2012), publisher: American Physical Society.
 - ¹⁵ K. Carva, M. Battiato, D. Legut, and P. M. Oppeneer, *Physical Review B* **87**, 184425 (2013), publisher: American Physical Society.
 - ¹⁶ G. Ju, A. Nurmikko, R. Farrow, R. Marks, M. Carey, and B. Gurney, *Physical Review B* **58**, R11857 (1998).
 - ¹⁷ M. Van Kampen, C. Jozsa, J. Kohlhepp, P. LeClair, L. Lagae, W. De Jonge, and B. Koopmans, *Physical review letters* **88**, 227201 (2002).
 - ¹⁸ M. Langner, C. Kantner, Y. Chu, L. Martin, P. Yu, J. Seidel, R. Ramesh, and J. Orenstein, *Physical review letters* **102**, 177601 (2009).
 - ¹⁹ M. Agranat, S. Anhitkov, A. Kirillin, V. Fortov, S. Anisimov, A. Granovskii, and P. Kondratenko, *JETP letters* **67**, 953 (1998).
 - ²⁰ A. Kirilyuk, A. V. Kimel, and T. Rasing, *Rev. Mod. Phys.* **82**, 2731 (2010).
 - ²¹ G. Li, K. Kushnir, Y. Dong, S. Chertopalov, A. M. Rao, V. N. Mochalin, R. Podila, and L. V. Titova, *2D Materials* **5**, 035043 (2018), publisher: IOP Publishing.
 - ²² C. La-o vorakiat, L. Cheng, T. Salim, R. A. Marcus, M.-E. Michel-Beyerle, Y. M. Lam, and E. E. M. Chia, *Applied Physics Letters* **110**, 123901 (2017), publisher: American Institute of Physics.
 - ²³ S. Kar, Y. Su, R. R. Nair, and A. K. Sood, *ACS Nano* **9**, 12004 (2015), publisher: American Chemical Society.
 - ²⁴ S. Kar, D. R. Mohapatra, E. Freysz, and A. K. Sood, *Physical Review B* **90**, 165420 (2014).
 - ²⁵ A. Tomadin, S. M. Hornett, H. I. Wang, E. M. Alexeev, A. Candini, C. Coletti, D. Turchinovich, M. Kläui, M. Bonn, F. H. Koppens, *et al.*, *Science advances* **4**, eaar5313 (2018).
 - ²⁶ S. Ruan, X. Lin, H. Chen, B. Song, Y. Dai, X. Yan, Z. Jin, G. Ma, and J. Yao, *Applied Physics Letters* **118**, 011102 (2021).
 - ²⁷ B. G. Alberding, G. P. Kushto, P. A. Lane, and E. J. Heilweil, *Applied Physics Letters* **108**, 223104 (2016), publisher: American Institute of Physics.
 - ²⁸ J. Neu and C. A. Schmuttenmaer, *Journal of Applied Physics* **124**, 231101 (2018).
 - ²⁹ H. Němec, F. Kadlec, and P. Kužel, *The Journal of Chemical Physics* **117**, 8454 (2002), publisher: American Institute of Physics.
 - ³⁰ H. Němec, F. Kadlec, C. Kadlec, P. Kužel, and P. Jungwirth, *The Journal of Chemical Physics* **122**, 104504 (2005), publisher: American Institute of Physics.
 - ³¹ H. Němec, F. Kadlec, S. Surendran, P. Kužel, and P. Jungwirth, *The Journal of Chemical Physics* **122**, 104503 (2005), publisher: American Institute of Physics.

- ³² P. Kužel, F. Kadlec, and H. Němec, The Journal of Chemical Physics **127**, 024506 (2007).
- ³³ E. Carpena, E. Mancini, C. Dallera, M. Brenna, E. Puppini, and S. De Silvestri, Phys. Rev. B **78**, 174422 (2008).
- ³⁴ T. Kampfrath, R. G. Ulbrich, F. Leuenberger, M. Münzenberg, B. Sass, and W. Felsch, Phys. Rev. B **65**, 104429 (2002).
- ³⁵ W. Fann, R. Storz, H. Tom, and J. Bokor, Physical Review B **46**, 13592 (1992).
- ³⁶ C.-K. Sun, F. Vallée, L. Acioli, E. Ippen, and J. Fujimoto, Physical Review B **50**, 15337 (1994).
- ³⁷ C. Suárez, W. Bron, and T. Juhasz, Physical review letters **75**, 4536 (1995).
- ³⁸ Y. Yang, S. Dal Forno, and M. Battiato, Journal of Infrared, Millimeter, and Terahertz Waves (2021), 10.1007/s10762-021-00815-5.
- ³⁹ C. L. Davies, J. B. Patel, C. Q. Xia, L. M. Herz, and M. B. Johnston, Journal of Infrared, Millimeter, and Terahertz Waves **39**, 1236 (2018).
- ⁴⁰ M. Naftaly and R. E. Miles, Journal of Applied Physics **102**, 043517 (2007).
- ⁴¹ A. D. Rakić, A. B. Djurišić, J. M. Elazar, and M. L. Majewski, Appl. Opt. **37**, 5271 (1998).

Appendix A: Detailed expression for PTMM

We assume here that the 0-th order component of the fields have been computed and is known in all the layers. We need to solve the Eqs. 8. The TMM is suited to solve Eqs. 8 in the absence of the source term $\mathcal{J}[z, \omega]$, but not when the term is different from 0.

The general solution of the non-homogeneous system can be constructed by computing the general solution of the associated homogeneous system and summing it to a particular solution. The general solution of the associated homogeneous system,

$$\begin{aligned}\partial_z E^{[1]}[z, \omega] &= -i\omega\mu[\omega]H^{[1]}[z, \omega], \\ \partial_z H^{[1]}[z, \omega] &= -i\omega\epsilon_T[\omega]E^{[1]}[z, \omega],\end{aligned}\quad (\text{A1})$$

is constructed using TMM.

We now have to construct any one particular solution to the non-homogeneous system. We write the source within a given layer in terms of its spatial Fourier components,

$$\mathcal{J}[z, \omega] = \sum_l \mathcal{J}[k_l, \omega] \exp[ik_l z], \quad (\text{A2})$$

where it should be noted that k_l is the spatial Fourier wavevector of the spatial distribution of the source term and not the light wavevector, therefore in general $k_l \neq \omega\sqrt{\epsilon\mu}$. For shortness in the following formulas we will drop the Fourier summation, to recover it only in the final expression.

We look for a particular solution in the form

$$E^{[1]}[z, t] = E e^{i(k_l z - \omega t)}, \quad (\text{A3})$$

$$H^{[1]}[z, t] = H e^{i(k_l z - \omega t)}, \quad (\text{A4})$$

By substituting in the Eqs. 8 we obtain the amplitudes of the fields for the particular solution,

$$k_l E = \mu\omega H, \quad (\text{A5})$$

$$ik_l H = i\epsilon\omega E + \mathcal{J}[k_l, \omega], \quad (\text{A6})$$

giving the particular solution,

$$\bar{F}[\omega, z] = \begin{bmatrix} E[\omega, z] \\ H[\omega, z] \end{bmatrix} = \mathcal{J}[k_l, \omega] \bar{b}[\omega, k_l, z], \quad (\text{A7})$$

with

$$\bar{b}[\omega, k, z] = \frac{i e^{ikz}}{\epsilon\mu\omega^2 - k^2} \begin{bmatrix} \omega\mu \\ k \end{bmatrix}. \quad (\text{A8})$$

We therefore write the general solution (recovering the summation on all the Fourier components of the source term) as,

$$\bar{F}[\omega, z] = \bar{a}[\omega, z] \bar{f}[\omega] + \sum_l \mathcal{J}[k_l, \omega] \bar{b}[\omega, k_l, z]. \quad (\text{A9})$$

Notice that the expression above is the solution to the inhomogeneous Maxwell's equation within a single layer: the interface conditions still need to be applied and the propagation through the multilayer still needs to be computed. This is however done following the same idea as in the TMM, and will not be addressed explicitly here.

Appendix B: Summary of the method

For the reader's convenience, we collect and summarise in this section the results of the whole developed approach.

We assume a multilayer, with layers numbered with $n = 1 \dots N$ and with known thicknesses d_n , sandwiched by two semi-infinite air regions (identified by the indices $n = 0$ and $n = N + 1$). We further assume that one or more of the layers are brought out of equilibrium by some means (which, notice, are not described here). We restrict ourselves to the case where only the Drude component of the dielectric response is modified by the out-of-equilibrium configuration, but allow for the materials to have a dielectric response which is the summation of a Drude part and background contributions $\epsilon_B[\omega]$ (which are however assumed not altered by the excitation). We assume that the Drude carrier density's n , and the Drude scattering rate's γ position and time dependence are perturbations of the equilibrium value,

$$\gamma[z, t] = \gamma^{[0]} + \gamma^{[1]}[z, t], \quad (\text{B1})$$

$$n[z, t] = n^{[0]} + n^{[1]}[z, t]. \quad (\text{B2})$$

We describe here only the propagation of electromagnetic waves through the layers with explicitly time-dependent material's properties only at normal incidence.

The fields E and H in each layer n can be constructed as a summation of a 0-th order and a 1-st order contribution:

$$\begin{bmatrix} E_n[\omega, z] \\ H_n[\omega, z] \end{bmatrix} \approx \begin{bmatrix} E_n^{[0]}[\omega, z] \\ H_n^{[0]}[\omega, z] \end{bmatrix} + \begin{bmatrix} E_n^{[1]}[\omega, z] \\ H_n^{[1]}[\omega, z] \end{bmatrix}. \quad (\text{B3})$$

Before proceeding, we remind that the fields are more conveniently expressed in terms of the right and left propagation wave intensities as,

$$\begin{bmatrix} E[\omega, z] \\ H[\omega, z] \end{bmatrix} = \bar{a}[\omega, z] \begin{bmatrix} f^{>}[\omega] \\ f^{<}[\omega] \end{bmatrix}, \quad (\text{B4})$$

where,

$$\bar{a}[\omega, z] = \begin{bmatrix} e^{i\omega\sqrt{\epsilon\mu}z} & e^{-i\omega\sqrt{\epsilon\mu}z} \\ -\sqrt{\frac{\epsilon}{\mu}}e^{i\omega\sqrt{\epsilon\mu}z} & \sqrt{\frac{\epsilon}{\mu}}e^{-i\omega\sqrt{\epsilon\mu}z} \end{bmatrix}. \quad (\text{B5})$$

The 0-th order component is calculated using standard TMM and gives that the wave intensities in any two layers n and m (including the seminfinite air regions on either side of the multilayer) are linked by the expression

$$\begin{bmatrix} f_m^{[0]>} \\ f_m^{[0]<} \end{bmatrix} = \bar{T}_{[n,m]} \begin{bmatrix} f_n^{[0]>} \\ f_n^{[0]<} \end{bmatrix}, \quad (\text{B6})$$

where

$$\bar{T}_{[n,m]} = \bar{a}_m^{-1}[0] \left(\prod_{j=m-1}^{n+1} \bar{a}_j[d_j] \bar{a}_j^{-1}[0] \right) \bar{a}_n[0]. \quad (\text{B7})$$

The above expression can be used to calculate, for instance, transmitted and reflected waves and, after that, the amplitudes of right and left moving waves in any layer.

For the 1-st order components, starting from Eq. 8, the general solution can be written as Eq. A9. Assuming that only the layer M ($n < M < m$) is excited with time-dependent properties. We obtain the wave intensities in any two layers n and m are linked by the expression,

$$\begin{bmatrix} f_m^{[1]>} \\ f_m^{[1]<} \end{bmatrix} = \bar{T}_{[n,m]} \begin{bmatrix} f_n^{[1]>} \\ f_n^{[1]<} \end{bmatrix} + \sum_l \mathcal{J}[k_l, \omega] \bar{T}_{[M,m]} \times (\bar{a}_N^{-1}[d_N] \bar{b}[\omega, k_l, d_N] - \bar{a}_N^{-1}[0] \bar{b}[\omega, k_l, 0]), \quad (\text{B8})$$

For simplicity, Eq. B8 can be written as,

$$\begin{bmatrix} f_m^{[1]>} \\ 0 \end{bmatrix} = \bar{T}_{[n,m]} \begin{bmatrix} 0 \\ f_n^{[1]<} \end{bmatrix} + \begin{bmatrix} J_M^{>} \\ J_M^{<} \end{bmatrix}. \quad (\text{B9})$$

Here $f_n^{[1]>}$ and $f_m^{[1]<}$ equal to zero because that the time-dependence of the material's properties will induce no variation to the incoming THz probe on the left or the absence of incoming radiation from the right. Based on this, the correction of the transmission will be

$$f_m^{[1]>} = J_M^{>} - \frac{\bar{T}_{[n,m],12}}{\bar{T}_{[n,m],22}} J_M^{<}. \quad (\text{B10})$$